ELSEVIER

Journal of Power Sources 63 (1996) 63–69

JOURNAL OF POWER SOURCES

Flooded flow fuel cells: a different approach to fuel cell design

U.B. Holeschovsky [1], J.W. Tester *, W.M. Deen

Energy Laboratory and Department of Chemical Engineering, Massachusetts Institute of Technology, 77 Massachusetts Avenue E40-455, Cambridge, MA 02139-4307, USA

Received 11 March 1996; revised 2 July 1996

Abstract

Flooded flow fuel cells provide a different approach to fuel cell design where gas phases are eliminated from the fuel cell structure by saturating the electrolyte with the reactant gases in separate vessels. The reactants are delivered to the electrode surface by passing the saturated liquid electrolyte across the electrode structure. This concept offers operational advantages over conventional porous-gas-diffusion electrodes, particularly for mobile applications where resistance to shock and vibration is desirable. The technical feasibility of the concept was evaluated by designing, constructing and operating an alkaline (KOH), H_2–O_2 fuel cell with flooded flow electrodes. Future work is focused on addressing important scale-up issues to increase current densities to commercially acceptable levels.

Keywords: Fuel cells; Design

1. Introduction

Most current types of fuel cell utilize porous-gas-diffusion (PGD) electrodes. A PGD electrode comprises a three-phase system: (i) a solid phase which is the electrode material; (ii) a liquid phase which is the electrolyte, and (iii) a gas phase for transport of the reacting components such as hydrogen or oxygen. During operation of a fuel cell, the reagent gases dissolve into the electrolyte, then diffuse to the electrode surface and finally react in the presence of a suitable catalyst on the electrode surface. The gas phase component cannot participate in the reaction itself, since it is neither an ion nor an electron conductor. Accordingly, the sole purpose of the gas phase is to supply reagent to the active interface between electrolyte and electrode.

As Meissner [1] proposed one could eliminate the gas phase from the fuel cell itself by saturating the liquid electrolyte with reagent gas. The reagent is then supplied to the electrode surface by passing the saturated electrolyte along the active electrode surface area. This operating mode with purposely flooded electrodes offers several advantages compared with conventional PGD-type fuel cells. The flux of the reactants to the reactive sites can be controlled and increased by increasing the electrolyte velocity. The entire surface area is supplied with reactants, whereas in PGD electrodes the reaction occurs over only a very narrow band of electrolyte located at the immediate vicinity of the gas–electrolyte meniscus. This inherent difference in active catalytic surface area promises to increase the practical current density levels (current per unit of electrode face area) and thus reduce costs for systems employing flooded flow (FF) electrodes.

Apart from the conceptual transport advantage of a single fluid phase, less complex electrode designs can be used in FF systems because of the removal of gas phases from the fuel cell structure. Uniformity of electrode porosity and spacing is less critical, as control of pressure to maintain a stationary gas–liquid interface inside the electrode is no longer needed. Thus, for FF systems, the use of sophisticated electrodes with dual porosity regions or Teflon-bonded components requiring rigid tolerances for size uniformity becomes unnecessary. Likewise, the formation of hot spots, inactive regions, and the possible hazards associated with the formation of an explosive mixture of hydrogen and oxygen are completely eliminated.

Without a gas–liquid interface in the fuel cell structure, more rugged systems are possible, less sensitive to shocks and vibrations. Due to the increased flux of reactants by the improved mass transfer to the active surface, the thickness of the electrode sheets can be increased, also contributing to the compactness and ruggedness of FF systems. Furthermore, cell temperature can be controlled easily as the required removal of the exothermic reaction enthalpy can be accomplished with high efficiency.

* Corresponding author.

[1] Current address: ARCO Chemical Company, PO Box 38007, South Charleston, WV 25303, USA.

Elsevier Science S.A.
PII S0378-7753(96)02443-3

This paper describes the first steps of evaluating the flooded flow concept using an alkaline fuel cell. We investigated current–voltage characteristics for operation of the anode and cathode separately in a three-electrode, half-cell apparatus with well-defined mass transfer conditions. We then combined the two half-cells to demonstrate the practical feasibility of a complete FF fuel cell. In passing, we note that there are a number of practical engineering issues that must be addressed before such a design would be acceptable for commercial applications. Operating current densities, *IR* losses, and parasitic pressure drops across fuel cell electrodes comprise the major issues for FF systems.

2. Experimental

Fig. 1 shows a schematic of the experimental setup for half-cell experiments. The first section is the half-cell assembly and the second is the saturator section for dissolving reactant gases. The two sections are linked by the electrolyte re-cycle, which is driven by two peristaltic pumps, one of which is operated with two pump heads. The electrolyte is saturated with gaseous feeds in two vessels connected in series.

Fig. 2 provides a schematic of the first stage saturator vessel. The vessel is a customized gas wash flask made of glass (Pyrex) with a volume of 500 ml. The major dimensions of the saturator are indicated in Fig. 2. Electrolyte inlet and outlet were added near the top and the bottom of the flask for circulation of electrolyte. The bottom of the gas dispersion tube was fitted with a 20 mm long fritted plate with pore sizes ranging between 20 and 50 μm. During operation, the saturator vessels are filled with electrolyte up to a level close to the bottle top as shown in Fig. 2. The gas inlet is connected to a gas tank with a pressure regulator. During operation a pressure of 0.2–0.3 bar above ambient was sufficient to finely disperse the gas into the electrolyte. After passing through the electrolyte, the gas is vented through the gas outlet located at the top of the gas dispersion tube.

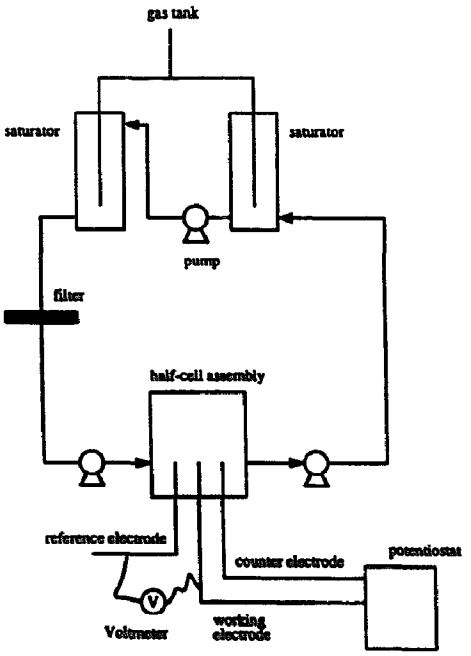

Fig. 1. Schematic of experimental setup for half-cell experiments.

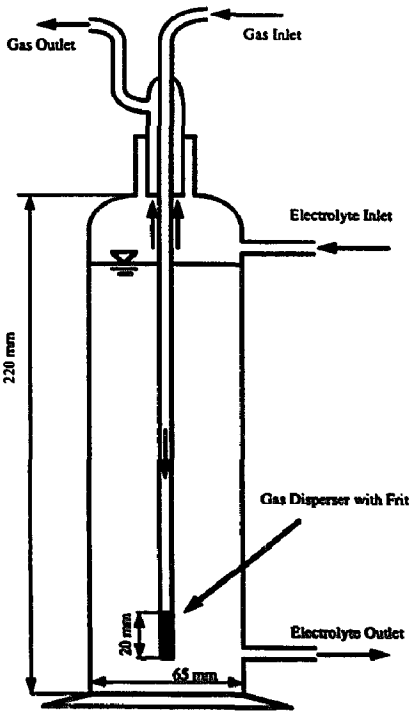

Fig. 2. Schematic of saturator.

The second stage saturator has the same height as the stage 1 saturator; however, the volume is only 250 ml compared with the 500 ml of the first stage saturator. Another difference is that the gas dispersion tube is shorter, so that the fritted bottom of the tube is at half the height of the vessel. The purpose of this configuration was to avoid the carry-over of gas bubbles in the exiting electrolyte. Two stages were used to assure complete saturation of the electrolyte. No differences in the experimental results were found when comparing experiments with a single-stage saturator to those experiments with two-stage saturation.

Fig. 3 shows a schematic of the half-cell assembly. The lower part of that figure details the flow channel containing the working electrode. The half-cell is contained in an open circular gas vessel (Pyrex) with a diameter of 70 mm and a height of 65 mm. This vessel is fitted with an electrolyte inlet and outlet as indicated in Fig. 3. A valve is attached on top of the inlet channel to allow for the removal of gas bubbles which may be carried over from the saturators. The counter electrode and a Luggin capillary connecting to the reference electrode are placed in the open glass cylinder. Up to four 50 mm × 50 mm platinum sheets and 0.1 mm thick were used as the counter electrodes. The Luggin capillary has a pointed tip

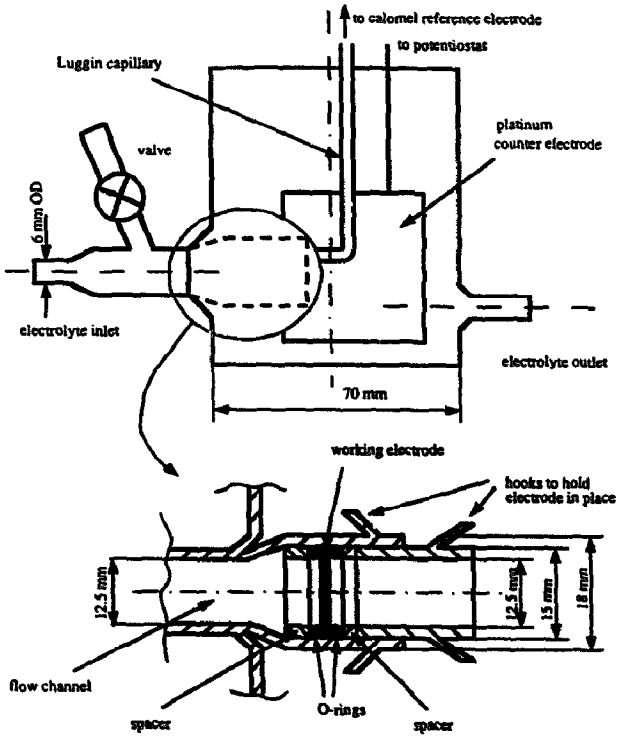

Fig. 3. Schematic of working electrode assembly.

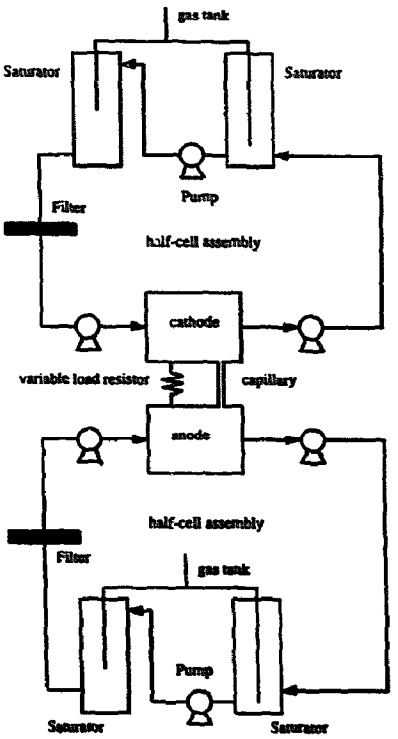

Fig. 4. Schematic of experimental setup for complete cell experiment.

and could be placed within about 1 mm of the working electrode.

The flow channel shown in the lower part of Fig. 3 has a conical section in which the inner diameter increases from 12.5 to 15 mm. A short glass tube, about 2 mm long with an inner diameter of 12.5 mm and an outer diameter slightly lower than 15 mm, can be slid into the flow channel. This short glass tube serves as a spacer and assures that the working electrode is placed perpendicular to the electrolyte flow. The working electrode, placed between two O-rings, is inserted into the flow channel and is pushed against the first spacer tube by a second spacer and a longer tube equipped with two hooks as shown in Fig. 3. To hold the spacer and electrode assembly in place, wires are wound around the hooks of the tube and two similar opposing hooks on the outside of the flow channel. By varying the thickness of the spacers, working electrodes of different thickness can be placed in the flow channel.

Fig. 4 shows a schematic of the experimental setup for complete cell experiments. This configuration consists of two separate half-cell cycles which are connected with a capillary. The capillary is filled with electrolyte and serves as an ion bridge. To complete the circuit, the anode and the cathode are connected by a variable load resistor. For the alkaline fuel cell systems studied in this investigation, the half-cell reaction taking place at the surface of the hydrogen electrode or anode is

$$2H_2 + 4OH^- \rightarrow 4H_2O + 4e^- \quad (1)$$

and at the oxygen electrode the half-cell reaction is

$$O_2 + 2H_2O + 4e^- \rightarrow 4OH^- \quad (2)$$

while the complete fuel cell reaction is the sum of both.

3. Results and discussion

The objective of this work was to demonstrate the feasibility of the FF fuel cell concept. The experiments were designed to establish a framework for understanding FF fuel cell operation and its limits. For this purpose screen electrodes were used, primarily because their surface area can be readily determined and varied. Furthermore, the simple geometry facilitates the modeling of FF cell operation. We recognize, at the outset, that screen electrodes will limit achievable current densities; but as a first step, we wanted to have a well-defined set of experimental conditions. For example, we examined cell performance using single and multiple, stacked screens, since this permits comparison of theoretical predictions and experimental results in the mass-transfer-limited operating regime. Results of half-cell and complete fuel cell experiments are also discussed.

3.1. Mass transfer to screens and packed beds of screens

This section summarizes correlations determined for mass transfer to screens and packed beds of screens. Using diffusivity and solubility data for oxygen in the electrolyte, the

mass transfer correlations were used to estimate current densities, thereby allowing us to compare our experimental results with theoretical calculations. Mass transfer to screens has significance for many practical applications. This problem has therefore been researched quite extensively. Coppola and Böhm [2] analyzed the available data for mass transfer across stacked screens, in terms of the Sherwood number (Sh), the Reynolds number (Re) and the Schmidt number (Sc). These quantities are defined as $Sh = kd/D$, $Re = Ud/\nu$, and $Sc = \nu/D$, where k is the mass transfer coefficient, d is the wire diameter, D is the reactant diffusivity, U is the superficial velocity, and $8{,}27O$ is the kinematic viscosity. The Sherwood number was empirically fitted to the following equation

$$Sh = ASc^{0.33}Re^{b} \quad (3)$$

where A and b are experimentally determined constants. The 0.33 exponent for Sc in Eq. (3) is the value expected from boundary-layer theory when the Peclet number, $Pe = Re \times Sc$, is large (see Section 4). Values for A and b as well as the methods used in their determination are summarized in Table 1. The values determined by different investigators are in relatively good agreement. The average value for the constant A is 0.82 with a standard deviation of 0.079 and the average value for the exponent b is 0.359 with a standard deviation of 0.034.

Values for mass transfer coefficients for single and stacked beds of screens are very similar. Satterfield and Cortes [6] found that 'mass transfer coefficients for multiple screen matrices were slightly lower than the single screen data'. Cano and Böhm [7] also report that mass transfer rates for packed beds are somewhat smaller than for single screens. In contrast to the above, Sioda [8] found that the mass transfer coefficients for 12-screen stacks were about 8% higher than mass transfer coefficients for single screens. Since the differences between single and multiple screens are relatively small and no clear trend is evident, the empirical correlations developed for multiple screens were averaged and also applied to single screens.

Table 1
Parameters for heat and mass transfer correlations for packed beds of screens (Eq. (3)) (adapted from Coppola and Böhm [2])

Investigators	Method	A	b
Coppage and London [3]	Heat transfer	0.731	0.356
Gay and Maugham [4]	Vaporization of mercury	0.846	0.298
Vogtländer and Bakker [5]	Electrochemical	0.773	0.415
Satterfield and Cortez [6]	Oxidation of hexane and toluene	0.865	0.352
Cano and Böhm [7]	Electrochemical	0.695	0.384
Sioda [9]	Electrochemical	0.904	0.360
Coppola and Böhm [2]	Electrochemical	0.838	0.37
Coppola and Böhm [2]	Electrochemical	0.908	0.34
Average values		0.82 ± 0.079 [a]	0.359 ± 0.034 [a]

[a] Indicates standard deviation.

3.2. Experiments with half-cells

Figs. 5 and 6 show typical potential versus current density semi-logarithmic plots for the cathode and anode for various flow velocities using a 90% platinum/10% iridium screen as

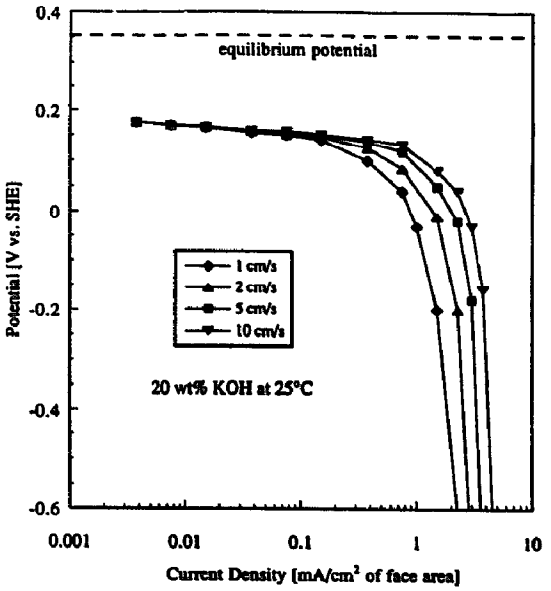

Fig. 5. Current–potential curves for oxygen reduction on 150 × 150 mesh screen (90% Pt/10% Ir) for various flow velocities.

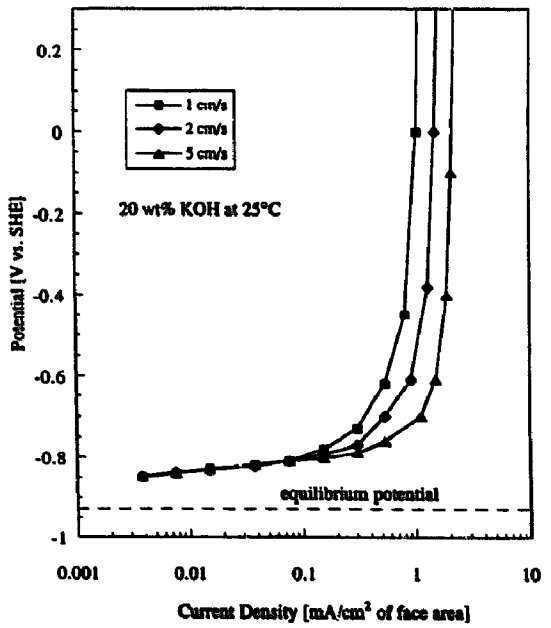

Fig. 6. Current–potential curves for hydrogen oxidation on a 150 × 150 mesh screen (90% Pt/10% Ir) for various flow velocities.

the electrode. The screens were 150 × 150 mesh plain weave, with a wire diameter of 0.0432 mm (Unique Wire Weaving, Hillside, NJ) and a ratio between internal surface area and face area of 1.6. The electrolyte used was a 20 wt.% KOH solution. The flow velocity was varied between 1 and 10 cm/s, the temperature of the electrolyte was approximately 23 °C, and the electrolytes were saturated using 1 atm of pure oxygen and hydrogen, respectively.

Figs. 5 and 6 show that for low current densities, the flow velocity does not affect the current–potential curve. Evidently, in this region, the overpotential is due to activation. Because the current density is low, only small concentration differences between bulk and electrode surface are necessary to provide the oxygen consumed at the electrode. Consequently, the concentration on the electrode surface equals the concentration in the bulk electrolyte. Improving mass transfer by increasing the flow velocity cannot increase the current density further since it is already at its kinetic limit.

As the current density is increased, the current–potential curves begin to diverge for different flow velocities. As flow velocity increases at a fixed potential, the measured current densities increase. In this region, the current densities are sufficiently high to reduce the oxygen concentration on the electrode surface. In the transition zone for intermediate current densities, the increased mass transfer extends the region in which activation overpotential dominates. As the current density is further increased, the potential drops abruptly. In this region, the surface concentration of reactant decreases to zero and the limiting current density is controlled by mass transfer.

The limiting current i_l under mass transfer control is determined by the transport of reactant through the diffusional boundary layer and is given by

$$i_l = knFAc_b \tag{4}$$

where n is the number of electrons transferred in the reaction, F is Faraday's constant, A is the cross-sectional area, and c_b is the bulk concentration. To compare experimental results for the limiting current density as defined in Eq. (4) with the mass transfer correlations listed in Table 1, we calculated the mass transfer coefficient from our limiting current data. This requires knowledge of the reactant solubility and diffusivity among other quantities. Since no data for the hydrogen diffusivity in KOH solutions are available, the following analysis was restricted to cathode experiments with oxygen.

3.2.1. Solubilities

Solubilities of gases in aqueous electrolytes are commonly described by using the Ostwald coefficient, L, defined as

$$L = \frac{V_g}{V_s} \tag{5}$$

where V_g is the volume of the gas adsorbed, and V_s is the volume of the absorbing solvent. Assuming the gas behaves ideally, the Ostwald coefficient is independent of the partial pressure of the gas and depends only on the temperature and liquid composition. The dependence of the Ostwald coefficient on the electrolyte concentration can be conveniently expressed by using the salting coefficient k_{sc} defined as

$$k_{sc} = \frac{\log(L^0/L)}{c_2} \tag{6}$$

where c_2 is the electrolyte concentration in mol/l, and the superscript (^{0}) refers to the pure solvent (water) without electrolyte present (note that log = base 10 logarithm). The salting coefficient reflects the change in solubility associated with the increase in concentration of a salt in water. For hydrogen and oxygen dissolved in KOH solution, the salting coefficient is positive, which means that the gases are less soluble over all temperatures of interest to this study. Consequently, the solubility of hydrogen or oxygen in pure water represents the upper bound on the solubility in an aqueous KOH solution. Battino [10] compiled the available data. Using the average Ostwald and salting coefficients, the average oxygen solubility was calculated to be 2.29×10^{-4} mol/l for a KOH concentration of 20 wt.% (4.24 M) at 25 °C. Agreement between the five investigators listed by Battino [10] is adequate, since the standard deviation for the oxygen concentration is ±2.9%.

3.2.2. Diffusivities

Gubbins and Walker [11] determined the oxygen diffusivity at 25 °C and at concentrations up to the solubility limit of KOH (51.7 wt.%). Davis et al. [12] determined the oxygen diffusivity at 25 °C up to a concentration of 34 wt.% and at 60 °C up to a concentration of 20 wt.%. Both research groups report a strong decrease in the diffusivity as KOH concentration is increased. At 25 °C and in pure water solution, Gubbins and Walker report a value of 1.9×10^{-5} cm^2/s and Davis et al. report a value of 1.95×10^{-5} cm^2/s, whereas for a 20% KOH solution they reported values are 1.0×10^{-5} and 0.84×10^{-5} cm^2/s, respectively. For our calculations, we used an average value of 0.92×10^{-5} cm^2/s.

When using Eq. (4), one has to take into account that the electrolyte is depleted of oxygen to some extent as it passes the screen electrode. The maximal current density (j_{max}) which the electrolyte can carry for a given flow velocity (V) is given by

$$j_{max} = VnFC_{sat} \tag{7}$$

where C_{sat} is the equilibrium solubility of oxygen in the electrolyte. As shown in Fig. 5, the limiting current density for a flow velocity of 1 cm/s was measured to be about 2.2 mA/cm^2 of face area. For this flow velocity, j_{max} is calculated to be 88 mA/cm^2 using Eq. (7). This means that only about 2.5% of the available oxygen was consumed. Therefore, the decrease in the oxygen bulk concentration as the electrolyte passes the electrode can be neglected for the calculation of the mass transfer coefficient. As the flow velocity increases, the assumption of constant bulk concentration becomes even better. For a flow velocity of 10 cm/s, j_{max} rises to 880 mA/cm^2 and the amount of available oxygen consumed is

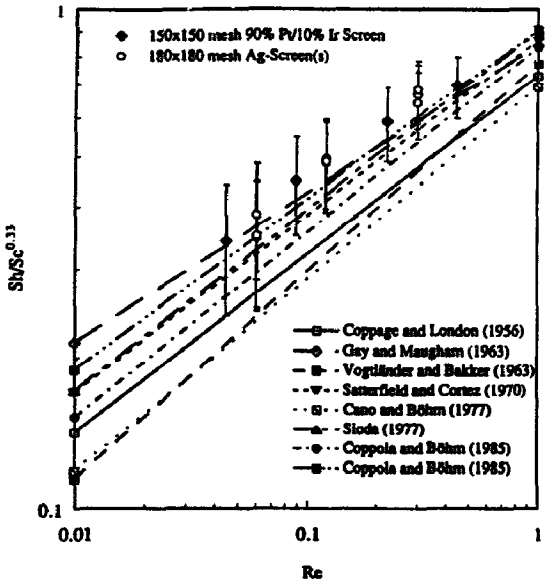

Fig. 7. Comparison of experimental results with mass transfer correlations. The ratio of the Sherwood number (Sh) to the cube root of the Schmidt number (Sc) as a function of the Reynolds number (Re).

only about 0.5%, since the higher current density is more than compensated for by a higher j_{max}. As a side note, these solubility-limited current density levels of order 10^2 to 10^3 mA/cm^2 of face area are quite acceptable for current commercial fuel cell applications.

Fig. 7 shows the comparison between our experimental results and the published correlations listed in Table 1. For illustration purposes, the results are plotted in terms of $Sh/Sc^{0.33}$ versus Re. Fig. 7 includes results for single screens and screen stacks (180×180 mesh silver). Experimental $Sh/Sc^{0.33}$ values determined from our limiting current data are generally higher than the ones calculated from the published correlations. However, since the experimental error bars clearly overlap into the band of correlations, one can conclude that the measured values are in good general agreement with these transport correlations. The error bars represent the propagated error in $Sh/Sc^{0.33}$. The maximal possible error in the face area of the working electrode is approximately 3%. The error in terms of the solubility is 2.9% which corresponds to the standard deviation of the available solubility data. The error in terms of the diffusivity was assumed to be 8.7% which corresponds to the deviation of the two reported values from their mean. The measurement error in terms of the limiting current was estimated to be 8%.

In addition to the good agreement with empirical correlations, the experimental data are consistent with theoretical predictions. Re in our experiments ranged from approximately 0.04 to 1 (Fig. 7), whereas Sc for oxygen was about 10^3. For small-to-moderate Re and large Sc, boundary-layer theory predicts that

$$Sh = APe^{1/3} = ASc^{1/3}Re^{1/3} \quad (8)$$

The observed exponent of Re in our experiments was 0.33, in excellent agreement with Eq. (8).

3.3. Experiments with complete cells

Fig. 8 shows the result for experiments with a complete fuel cell. This cell consisted of two separate electrolyte recycle loops which were joined by a glass capillary, as shown in Fig. 4. One recycle was saturated with oxygen whereas the second recycle was saturated with hydrogen. Single 150×150 mesh screens (90% Pt/10% Ir) were used in both half-cells. To allow comparison with half-cell experiments, the experimental parameters were the same as in the half-cell experiments.

The results for the complete cell are in very good agreement with the corresponding half-cell experiments shown in Figs. 5 and 6. In the low current density region, the potential of the complete cell is approximately equal to the difference between the cathode potential and the anode potential. The drop of the potential occurs at the same current density, depending on which half-cell recycle is limiting. Fig. 8 shows results of experiments in which the flow velocities were adjusted to establish the limiting current density on both anode and cathode. This means that a decrease in flow velocity of either recycle would potentially reduce the limiting current density, but a further increase in fluid recycle velocity would not increase the limiting current density.

Two examples are shown in Fig. 8. For a catholyte flow velocity of 5 cm/s, the flow velocity of the anolyte needs to be 9.6 cm/s, and for a catholyte velocity of 1.1 cm/s, the anolyte flow velocity needs to be 2 cm/s to achieve simultaneously limiting operation. The ratio of the corresponding flow velocities for operation at which anode and cathode are simultaneously limiting is approximately 1.87.

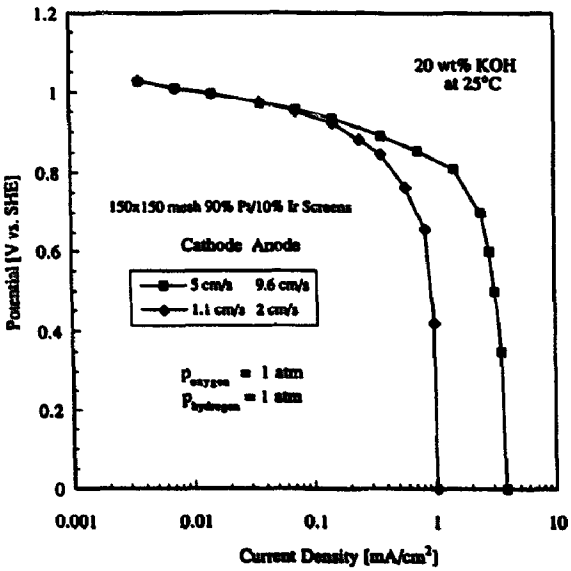

Fig. 8. Current–potential curve of complete flooded flow cell.

The difference in the flow velocities can be explained by considering the stoichiometry of the reaction in conjunction with the solubilities of oxygen and hydrogen. For a 20 wt.% KOH solution at room temperature, the solubility of hydrogen and oxygen are very similar, e.g. 0.23 mol/m^3 for oxygen and 0.22 mol/m^3 for hydrogen [13]. Each oxygen molecule receives 4 electrons and each hydrogen molecule yields two electrons when reacting to water. Thus, if solubility and stoichiometry were the only relevant parameters, one would expect the ratio of catholyte to anolyte velocity to be approximately 2, which is very close to the experimentally observed ratio of 1.87.

A complete analysis needs to take into account the difference in the diffusivities of oxygen and hydrogen in the electrolyte solution. Since no data for the diffusivity of hydrogen in KOH solutions are available, the argument is qualitative. The hydrogen diffusivity in pure water is approximately two times higher than the oxygen diffusivity (3.8×10^{-5}cm^2/s versus 1.95×10^{-5}cm^2/s). For oxygen, the diffusion coefficient decreases strongly as the KOH concentration increases. For example, in a 20 wt.% KOH solution it is 50% lower than in pure water, and in a 45 wt.% solution it is 90% lower. Similar effects can be expected for hydrogen, although the magnitude of the decrease in the diffusion coefficient will probably be different. In general, we expect the hydrogen diffusion coefficient to be larger than the oxygen diffusion coefficient. This will tend to decrease the difference in the limiting current density for oxygen reduction and hydrogen oxidation, which is consistent with our experimental results.

We also experimented with a mixed feed configuration. This setup is characterized by a single electrolyte recycle. After being saturated with oxygen and hydrogen in separate saturators, catholyte and anolyte were mixed and passed through screens of different materials, e.g. platinum and silver. Preliminary experiments by Meissner [1] showed that when passing a mixed feed through a silver screen electrode in FF operation, the potential measured corresponded to the cathodic potential, suggesting that oxygen may react selectively at the silver electrode, with substantially no hydrogen consumption. Similarly, if the mixed feed is passed through a platinum electrode, the measured potential corresponded to the hydrogen anode, suggesting that a platinum electrode could serve selectively as the hydrogen anode. We were successful in repeating these findings; however, upon connecting the platinum and silver screen, the open-circuit potential difference disappeared gradually and continuous operation was not possible.

4. Conclusions

Our experiments demonstrate that FF fuel cells are technically feasible. The measured current density potential curves are in general agreement with theoretical expectations. For current densities less than 0.1 mA/cm^2, the flow velocity has no effect on the current density. For higher current densities, an increase in flow velocity increases the limiting current density and extends the kinetically-limited operating regime. Consequently, FF operation allows control of the limiting current density through the flow velocity. For a given flow velocity, the hydrogen half-cell was found to be limiting, which follows from the stoichiometry and the solubilities of hydrogen and oxygen. In a separate feed configuration, the flow velocities of the catholyte and anolyte can be independently varied to optimize use of the available surface area of each half-cell. Theoretical values calculated from mass transfer correlations are in excellent agreement with the experimental results in the mass-transfer-limited region.

To demonstrate the FF concept we used screen electrodes. The advantage of using screens as electrodes is their simple geometry with known internal surface areas, which facilitated the modeling of transport under FF conditions and simplified the experimental setup for making a direct comparison with theoretical predictions. However as we mentioned earlier, the internal surface areas of screens are too low to support current densities of conventional practical fuel cells which are of the order of 100 mA/cm^2 or more. To find out if the current densities in FF fuel cells can be competitive with conventional fuel cells, we have experimented with high internal surface area electrodes and will report results in a forthcoming paper where *IR* losses and electrode pressure drop issues are addressed.

Acknowledgements

The authors would like to thank M-C Power Corporation and the MIT Energy Laboratory for partial financial support of the project. We are especially grateful to the late Herman P. Meissner, the inventor of the flooded flow fuel-cell concept, for his contributions, advice and encouragement during the early stages of this research. We would like to acknowledge Frank Schora for his interest and encouragement. Finally we would like to thank Alan Hatton, Ronald Latanision and Donald Sadoway for their helpful discussions and suggestions.

References

[1] H.P. Meissner, *Pend. Patent Applic., Nov. 1989.*
[2] L.U. Coppola and U. Böhm, *Chem. Eng. Sci., 40* (1985) 1594.
[3] J.E. Coppage and A.L. London, *Chem. Eng. Prog., 52* (1956) 57.
[4] B. Gay and R. Maugham, *Int. J. Heat Mass Transfer, 6* (1963) 277.
[5] P.H. Vogtländer and C.A.P. Bakker, *Chem. Eng. Sci., 18* (1963) 583.
[6] C.N. Satterfield and D.H. Cortez, *Ind. Eng. Chem. Fundament., 9* (1970) 613.
[7] J. Cano and U. Böhm, *Chem. Eng. Sci., 32* (1977) 213.
[8] R.E. Sioda, *Electrochim. Acta, 22* (1977) 439.
[9] R.E. Sioda, *J. Electroanal. Chem., 70* (1976) 49.
[10] R. Battino, *Solubility Data Series*, Vol. 7, Pergamon, Oxford, 1981.
[11] K.E. Gubbins and R.D. Walker, Jr., *J. Electrochem. Soc., 12* (1965) 469.
[12] R.E. Davis, G.L. Horvath and C.W. Tobias, *Electrochim. Acta, 12* (1967) 287.
[13] C.L. Young, *Hydrogen and Deuterium*, Vol. 5-6, Pergamon, Oxford, 1981.